Hindawi
Geofluids
Volume 2022, Article ID 4023435, 14 pages
https://doi.org/10.1155/2022/4023435

Research Article

Study on the Wettability and Spontaneous Imbibition Characteristics of Lacustrine Shale

Haitao Xue,[1,2,3] Guozhi Ding,[3] Zhentao Dong,[3] Rixin Zhao,[3] Ce An,[3] Boheng Li,[3] Yuan Zhou,[3] Penglei Yan,[3] Jinliang Yan,[3] Chunlei Li,[3] and Yuxi Jin[4]

[1]*State Key Laboratory of Shale Oil and Gas Enrichment Mechanisms and Effective Development, Beijing 100083, China*
[2]*National Energy Shale Oil Research and Development Center, Beijing 100083, China*
[3]*School of Geosciences, China University of Petroleum (East China), Qingdao 266580, Shandong, China*
[4]*Asian Infrastructure Investment Bank, Beijing 100101, China*

Correspondence should be addressed to Zhentao Dong; b20010024@s.upc.edu.cn

Received 8 October 2021; Revised 1 December 2021; Accepted 4 January 2022; Published 10 February 2022

Academic Editor: Shengnan Nancy Chen

Copyright © 2022 Haitao Xue et al. This is an open access article distributed under the Creative Commons Attribution License, which permits unrestricted use, distribution, and reproduction in any medium, provided the original work is properly cited.

Wettability plays a significant role in the exploration and development of shale oil. The wettability affects the oil enrichment and restricts the selection of fracturing fluids. Shale is composed of complex minerals and organic matter. The pores composed of inorganic minerals have water wettability, while the pores composed of organic matter show the characteristics of oil wetting. The contact angle experiment and the spontaneous imbibition experiment are the most commonly used methods for characterizing wettability. The Qingshankou Formation in the Songliao Basin has thick source rocks, which is a favorable interval for shale oil exploration and development. Strengthening the wettability research in this area is of great significance for the exploration of shale oil. The wettability of different lithofacies shale in the northern Songliao Basin is seldom characterized, and there is a lack of comparative studies on contact angle and imbibition characteristics. In view of this situation, the shale of the Qingshankou Formation in the northern Songliao Basin has been classified. This article used the method of spontaneous imbibition combined with nuclear magnetic resonance to characterize the wettability of shale and analyze the influencing factors of the wettability of different shale lithofacies. Six samples with different lithological characteristics were used for this experiment. The study found that the imbibition results of samples with different lithofacies are different. The imbibition of sandy interlayer is less affected by the direction, while the imbibition of shale is more affected by the direction. The water imbibition volume of the sample is related to the content of clay minerals. The relationship of water imbibition volume in different lithofacies samples is as follows: low organic matter laminated siliceous shale > high organic matter massive clay shale > sandy interlayer > high organic matter laminated siliceous shale > high organic matter massive siliceous shale. Excessive content of clay minerals will cause shale to absorb water and expand and block pores, which is not conducive to further water imbibition by shale. The volume of oil imbibed is related to the organic carbon content. The relationship of oil imbibition volume in different lithofacies samples is as follows: high organic matter massive clay shale > high organic matter laminated siliceous shale > sandy interlayer > low organic matter laminated siliceous shale > high organic matter massive siliceous shale. The higher the total organic carbon content, the more developed the lipophilic pore network, and the more the volume of oil imbibed by the sample.

1. Introduction

Wettability describes the properties of the interface between different phases. In reservoir engineering, wettability shows the tendency of reservoir rock surfaces to be preferentially wetted by a fluid phase [1, 2]. Shale oil reservoir wettability refers to the tendency of oil to expand or adhere to the surface of inorganic minerals or kerogen pores in shale reservoirs [3, 4]. Wettability plays a vital role in the exploration and development of shale oil by affecting the enrichment and flow of oil in shale reservoirs. The wettability of shale determines the affinity of the surface for oil and water, which affects the ratio of free shale oil in the pores of organic matter and inorganic minerals. It is an important

parameter to accurately estimate the movable resources of shale oil. Shale oil development requires extensive hydraulic fracturing of shale oil reservoirs. However, the reflux efficiency of fracturing fluid in some shale oil reservoirs is too low, which dramatically increases the cost of shale oil development. Therefore, the problem of shale fracturing fluid loss has attracted the attention of a large number of scholars [5–10]. The academic circles generally believe that wettability is the main factor affecting the water spontaneous imbibition of shale and the primary mechanism that causes excessive water imbibition of shale. Studying the wettability of shale oil reservoirs is extremely important for selecting suitable fracturing fluids and improving oil and gas recovery [11–16].

Shale is composed of complex minerals and organic matter, including brittle minerals (quartz, feldspar, and calcite) and clay minerals [17–19]. The current general opinion is that inorganic minerals are water wettability under the original reservoir conditions, while the organic matter is oil wettability [20–23]. The type of kerogen will affect the oil wettability of organic matter. It makes the characterization of shale wettability extremely complicated [24]. The pore composition and connectivity of shale are complex [25–28]. Generally speaking, pores composed of inorganic minerals are hydrophilic, and pores distributed in organic matter are lipophilic [29]. The higher the maturity of organic matter, the stronger the lipophilicity [30]. The simultaneous appearance of inorganic water-wet macropores and organic oil-wet small pores makes shale have double wettability, which is also where the wettability of shale oil reservoirs is different from that of conventional reservoirs [31].

The contact angle experiment and the spontaneous imbibition experiment are the most commonly used methods for characterizing wettability. Engelder et al. [32] measured the oil and water/brine contact angles of Marcellus and Haynesville shale samples under air to characterize the wettability of the shale. Mokhtari et al. [33] measured the contact angle of deionized water at ambient room temperature and pressure on the surface of Eagle Ford, Mancos, Bakken, Niobrara, and Green River shale samples. They analyzed the correlation between the contact angle and the total organic carbon content. Borysenko et al. [34] studied the contact angle and spontaneous imbibition behavior of two shales with different wettability (Bass Basin and Continental Officer Basin), and some pure minerals or their mixtures. Liang et al. [35] studied the wettability of organic-rich shale samples from the Longmaxi Formation (LF) in China through contact angle and spontaneous imbibition experiments. Takahashi and Kovscek [36] conducted spontaneous countercurrent spontaneous imbibition experiments on low-permeability siliceous shale core samples to study the influence of the PH value of different types of brine on wettability. Dehghanpour et al. [37] studied the wettability of shale in Fort Simpson (FS), Muskwa (M), and Otter Park (OP) in Horn River Basin (HRB) and measured the contact angle of oil and water in the air on the shale surface, and a spontaneous imbibition experiment was carried out using intact shale samples. However, the wettability results of shale obtained by spontaneous imbibition experiments often contradict the results obtained by contact angle experiments [37, 38]. This is because the spontaneous imbibition experiment focuses on the average wettability of the entire core, while the contact angle experiment shows the wettability of a particular surface. The spontaneous imbibition experiment combined with nuclear magnetic resonance can dynamically monitor the amount of liquid imbibed by the shale, the priority order of liquid imbibition pore throats [39], and reveal the imbibition mechanism and the influencing factors of wettability of the shale [40].

Lithofacies comprehensively reflect rock characteristics such as mineral composition, organic matter, and pore structure [41]. However, the wettability of different lithofacies shale in the northern Songliao Basin is less characterized, and there is a lack of comparative studies on contact angle and spontaneous imbibition. In view of this situation, the shale of the Qingshankou Formation in the northern Songliao Basin has been classified. Six samples with different lithological characteristics were used for this experiment. The experiment uses contact angle measurement, spontaneous imbibition combined with nuclear magnetic resonance method, to characterize the wettability of shale with different lithofacies characteristics and analyze the influencing factors of the wettability of different lithofacies shale.

2. Methodologies

2.1. Geological Background and Sample Information. The area of this study is consistent with our previous study on using contact angle to characterize the wettability of shale [42]. The Songliao Basin in Northeast China is a Cretaceous continental rift basin. The Qingshankou Formation was deposited in the postcracking thermal subsidence stage. The thickness of the stratigraphic group is usually in the range of 200–500 m. The lithology and lithofacies vary greatly. The lithology in the Qijia-Gulong sag is a thick lacustrine dark brown mud shale, while the lithology at the edge of the sag is an interbedded shale and sandstone [43, 44]. The main lithology is dark brown mud shale with a small amount of oil shale, which is a favorable layer for shale oil exploration and development. According to the change of lithofacies, the Qingshankou Formation can be divided into 3 sections. The target interval of this study is the first member of the Qingshankou Formation. During the deposition of the first member of Qingshankou Formation, the lake basin expanded to the largest extent. A set of gray-black mudstone, oil shale, and gray-white silty fine sandstone with varying thicknesses were deposited in the basin [45].

In this study, cores were taken from the different depth sections. The samples were analyzed for whole-rock minerals, TOC, and thin rock sections. Thin-section observations show that the Qingshankou Formation shale in the northern Songliao Basin has various structural features such as layered, laminar, and yellow massive (Figure 1). The lithofacies type, organic matter abundance, XRD whole-rock minerals, and clay mineral analysis results of the samples are

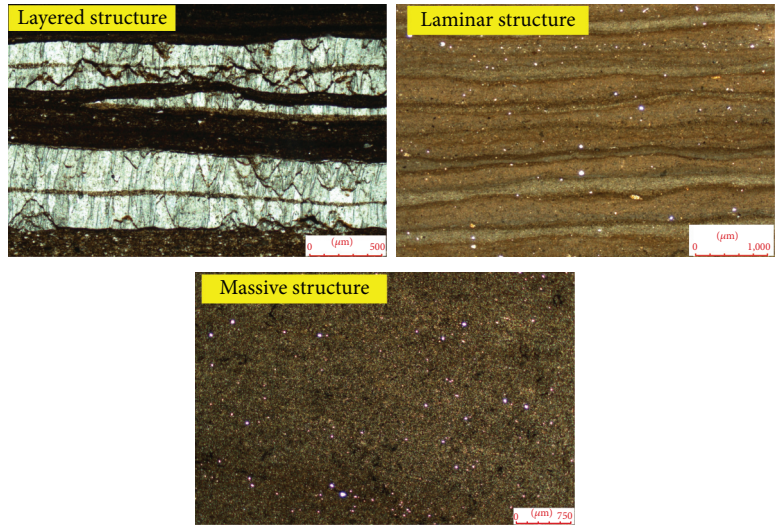

Figure 1: Structure characteristics of shale oil reservoir samples [45].

shown in Table 1. This lithofacies classification is based on Liu Bo's classification scheme for mud shale in Qingshankou Formation in the southern Songliao Basin, using a four-component three-terminal classification method, fully considering the sample's macrostructure, organic matter content, and mineral composition. There are three representative lithofacies: sandy interlayer (YY-72-2) has high siliceous mineral content, low clay mineral content, and low TOC. Low organic matter laminated siliceous shale (YJ-62-3) has a higher content of siliceous minerals, a higher content of clay minerals, and a higher TOC. High organic matter massive clay shale (YJ-27-1) has low siliceous mineral content, high clay mineral content, and high TOC.

2.2. Experimental Method

2.2.1. Sample Processing

(1) Contact Angle Experiment Sample. The surface roughness will have a significant impact on the measurement of contact angle [46]; it is necessary to pretreat the sample surface to eliminate this effect. The surface of the sample was polished by 400, 800, 1500, and 2000 mesh grinding wheels in sequence. When Ra is less than 0.5 μm, the surface of the sample can be regarded as approximately smooth. Ra is the arithmetic mean of the absolute value of the distance from each point on the measured contour to the reference line within the sampling length L, and its size can be used to characterize the roughness of the sample surface [42, 46].

(2) Spontaneous Imbibition NMR Experiment Sample. Use a wire cutter to cut each sample into four cylindrical samples with a length of 10 mm and a diameter of 25 mm. Two of them were cut along the direction of the vertical bedding plane, and two were cut along the direction of the parallel bedding plane (Figure 2) [38, 47]. Samples 1 and 2 have parallel bedding for oil imbibition and water imbibition, respectively; samples 3 and 4 have vertical bedding for oil imbibition and water imbibition, respectively.

The original column sample contains a certain amount of colloidal asphaltene, which blocks the pore throat and affects the process of spontaneous fluid infiltration into the pore throat. It is necessary to perform an oil washing operation before the spontaneous imbibition and nuclear magnetic resonance experiment of the sample. This oil washing operation uses the DY-6 high-efficiency oil washing instrument; the washing oil solvent is a 4 : 1 alcohol-benzene mixed solvent. The heating temperature is set to 70°C, the pressure is set to 1 MPa, and the oil washing time is 72 hours. After the oil washing process was completed, the sample was taken out, and some samples were damaged. The pore volume of the damaged sample cannot be obtained by calculation, and only the complete sample is selected for drying. The complete sample is selected and put in the drying box for drying treatment, the temperature is set to 70°C, and the time is set to 72 hours. The diameter and length of the complete sample are remeasured. The porosity of the complete sample is measured using the helium porosimetry method. To ensure that only the bottom surface of the sample touches the imbibed fluid during the imbibition process, apply epoxy resin around the cylinder sample, leaving only the upper and lower bottom surfaces. The treated samples were divided into two groups: one group was used to imbibe n-dodecane, and the other group was used to imbibe deionized water (Figure 3 and Table 2).

2.2.2. Experimental Process

(1) Contact Angle Experiment. The testing instrument is the JC2000D contact angle measuring instrument produced by Shanghai Zhongchen Company. The instrument includes two parts: the CCD optical system and the stage control system. Contact angle measurement range: 0–180°, contact angle measurement resolution: 0.01°.

Table 1: Basic geochemical parameters and mineral composition information of samples.

Lithofacies type	Sample number	Formation	TOC (%)	Siliceous mineral (%)	Calcareous minerals (%)	Calcareous minerals (%)
Sandy interlayer	YY-72-2	K2qn1	0.64	76.9	3.0	20.1
Low organic matter laminated siliceous shale	YG-616-3	K2qn1	0.70	62.2	12.1	25.6
Low organic matter laminated siliceous shale	YJ-62-3	K2qn1	0.99	58.6	16.4	25
High organic matter laminated siliceous shale	YA-151-1	K2qn1	2.88	51.6	11.6	36.8
High organic matter massive siliceous shale	YD-22-1	K2qn1	3.95	58.2	7.9	33.9
High organic matter massive clay shale	YJ-27-1	K2qn1	4.33	18.1	1.9	80

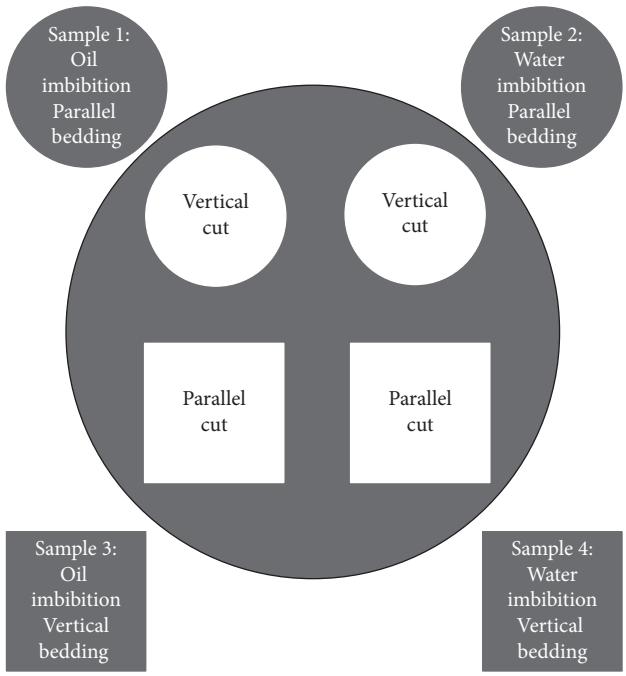

Figure 2: Shale oil reservoir sample cutting method.

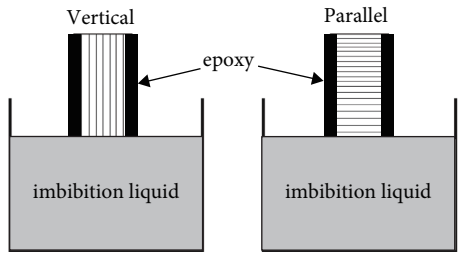

Figure 3: Bedding surface and bottom surface direction.

Experimental procedure is as follows. ① Through the control software, use a microsyringe to drop a droplet on a smooth, clean, and horizontally placed mineral surface. The size of the droplet is only 2-3 microliters to eliminate the influence of gravity on the shape of the droplet. ② After the droplet contact angle is stable, use the camera to photograph the shape of the droplet on the mineral surface. ③ Use the image processing software that comes with the instrument to analyze and measure the left contact angle, right contact angle, and the average value of the contact angle of the droplet on the mineral surface. ④ Group samples were subjected to 3-4 repeated measurements, and the average value of the contact angle was obtained.

(2) Spontaneous Imbibition NMR Experiment. The nuclear magnetic resonance experiment instrument is MicroMR12-025V nuclear magnetic resonance analyzer. The experiment is divided into the n-dodecane imbibition experiment group and the deionized water imbibition experiment group. The process of the n-dodecane imbibition experiment group is as follows. ① The quality and nuclear magnetic signal of the dried sample were measured after pretreatment. ② The sample was immersed in n-dodecane containing an evaporating dish. ③ The changes in the imbibition quality of the sample and the amount of imbibition NMR signal were collected. Previous core imbibition experiments have shown that the imbibition velocity is very high at the initial stage, and then the velocity becomes smaller until the imbibition velocity drops to zero [47]. Therefore, the collection time interval in the early stage is short, and the collection time interval in the later stage is appropriately extended. ④ When the imbibition quality of the sample and the nuclear magnetic signal appear unchanged or decreased for three times, it is deemed that the imbibition is completed. ⑤ The sample after the imbibition is put into the vacuum pressure saturation device for pressure saturation for 72 h. ⑥ The quality and NMR signal of the sample were measured when pressure saturation is completed.

The experimental process of the deionized water imbibition experiment group is roughly the same as that of the n-dodecane imbibition experiment group, but the deionized water imbibition experiment group did not perform saturated water. The reason is that the samples selected in this experiment contain a lot of clay minerals, and when the shale is pressurized and saturated with water, the shale is easy to fragment [48].

2.3. Data Processing. The spontaneous imbibition curve records the change law of sample imbibition over time, reflecting the pore characteristics of the rock, the

Table 2: Spontaneous imbibition sample information.

Experimental group	Lithofacies type	Sample number	Bedding surface and bottom surface direction	Column length (mm)	Column diameter (mm)	Porosity (%)
N-dodecane imbibition experiment	High organic matter laminated siliceous shale	YA-151-1	Parallel	10.67	25.23	9.00
	Sandy interlayer	YY-72-2	Parallel	13.98	25.19	11.89
		YY-72-2	Vertical	10.41	25.28	9.10
	Low organic matter laminated siliceous shale	YG-616-3	Parallel	13.08	24.33	9.71
	High organic matter massive siliceous shale	YD-22-1	Parallel	7.78	25.47	3.00
	High organic matter massive clay shale	YJ-27-1	Parallel	11.01	25	7.01
		YJ-27-1	Vertical	12.13	25.12	8.00
	Low organic matter laminated siliceous shale	YJ-62-3	Parallel	12.17	25	3.82
		YJ-62-3	Vertical	10.51	25.32	5.4
Deionized water imbibition experiment	High organic matter laminated siliceous shale	YA-151-1	Parallel	10.55	25.03	9.00
		YA-151-1	Vertical	11.72	26.56	8.32
	Sandy interlayer	YY-72-2	Parallel	11.77	25.51	11.89
		YY-72-2	Vertical	10.53	25.82	9.10
	Low organic matter laminated siliceous shale	YG-616-3	Parallel	9.1	24.43	9.71
	High organic matter massive siliceous shale	YD-22-1	Parallel	19.88	25.52	3.00
	High organic matter massive clay shale	YJ-27-1	Parallel	11.23	25.22	7.01
		YJ-27-1	Vertical	10.93	25.19	8.00
	Low organic matter laminated siliceous shale	YJ-62-3	Parallel	11.63	25.39	3.82
		YJ-62-3	Vertical	11.08	25.48	5.40

interaction mechanism between the rock and the fluid, and so on. There is a difference between rocks with different lithofacies. In order to focus on the influence of lithofacies on the imbibition characteristics, it is necessary to remove the effect of pore volume on imbibition. Therefore, the quality of imbibed liquid m_l is converted into the percentage C of the volume of imbibed liquid V_l in the pore volume V_p of the sample. The specific calculation process is as follows:

$$V_p = \phi \pi r^2 h,$$
$$V_l = \frac{m_l}{\rho_l}, \quad (1)$$
$$C = \frac{V_l}{V_p},$$

where V_p is the pore volume of the column sample, ml; V_l is the volume of the imbibed liquid, ml; C is the percentage of the volume of imbibed liquid in the pore volume of the column sample; C_o is the percentage of oil imbibition volume in the pore volume of the column sample; C_w is the percentage of imbibed water volume in the pore volume of the column; r is the radius of the bottom surface of the column, mm; h is the height of the column, mm; Φ is the porosity of the column sample (%); m_l is imbibed liquid quality, mg; and ρ_l is imbibed liquid density, 10^{-3} g/cm^3.

In this experiment, the density of deionized water is 1 g/cm^3 and the density of n-dodecane is 0.753 g/cm^3.

3. Results and Discussion

3.1. Contact Angle. The average value of the "gas-water-rock" contact angle of the six selected samples with different lithofacies characteristics is shown in Table 3. From the table, it can be seen that the "gas-water-rock" contact angle of the low organic shale is far lower than the high organic shale, and the contact angle of the sandy interlayer (YY-72-2) is much smaller than that of other samples. The reason is that the high organic content makes the sample more lipophilic, the sandy interlayer (YY-72-2) sample has a higher permeability, and the water droplets penetrate the surface.

3.2. Spontaneous Imbibition

3.2.1. The Difference of Imbibition along the Vertical and Parallel Bedding Directions. The water imbibition rate and final imbibition volume of the samples will be affected by the bedding. For sandy interlayer and shale, the vertical bedding plane's imbibition rate and final imbibition volume are greater than those of the parallel bedding plane. Figure 4(a) is the comparison of the water imbibition curves of the parallel bedding and the vertical bedding of the sandy interlayer sample (YY-72-2). The bedding structure of the sandy interlayer sample is not well developed, and the water imbibition rate of the parallel bedding plane and the vertical bedding plane is not much different, but the final imbibition volume is different. The water imbibition of the parallel bedding plane is significantly less than that of the vertical bedding plane. Figures 4(b) and 4(c) are the comparison of

Table 3: Average values of "gas-water-rock" contact angle for different petrographic.

Lithofacies type	Sample number	"Gas-water-rock" contact angle
Sandy interlayer	YY-72-2	8.10
Low organic matter laminated siliceous shale	YG-616-3	23.58
Low organic matter laminated siliceous shale	YJ-62-3	28.40
High organic matter laminated siliceous shale	YA-151-1	41.30
High organic matter massive siliceous shale	YD-22-1	40.68
High organic matter massive clay shale	YJ-27-1	47.69

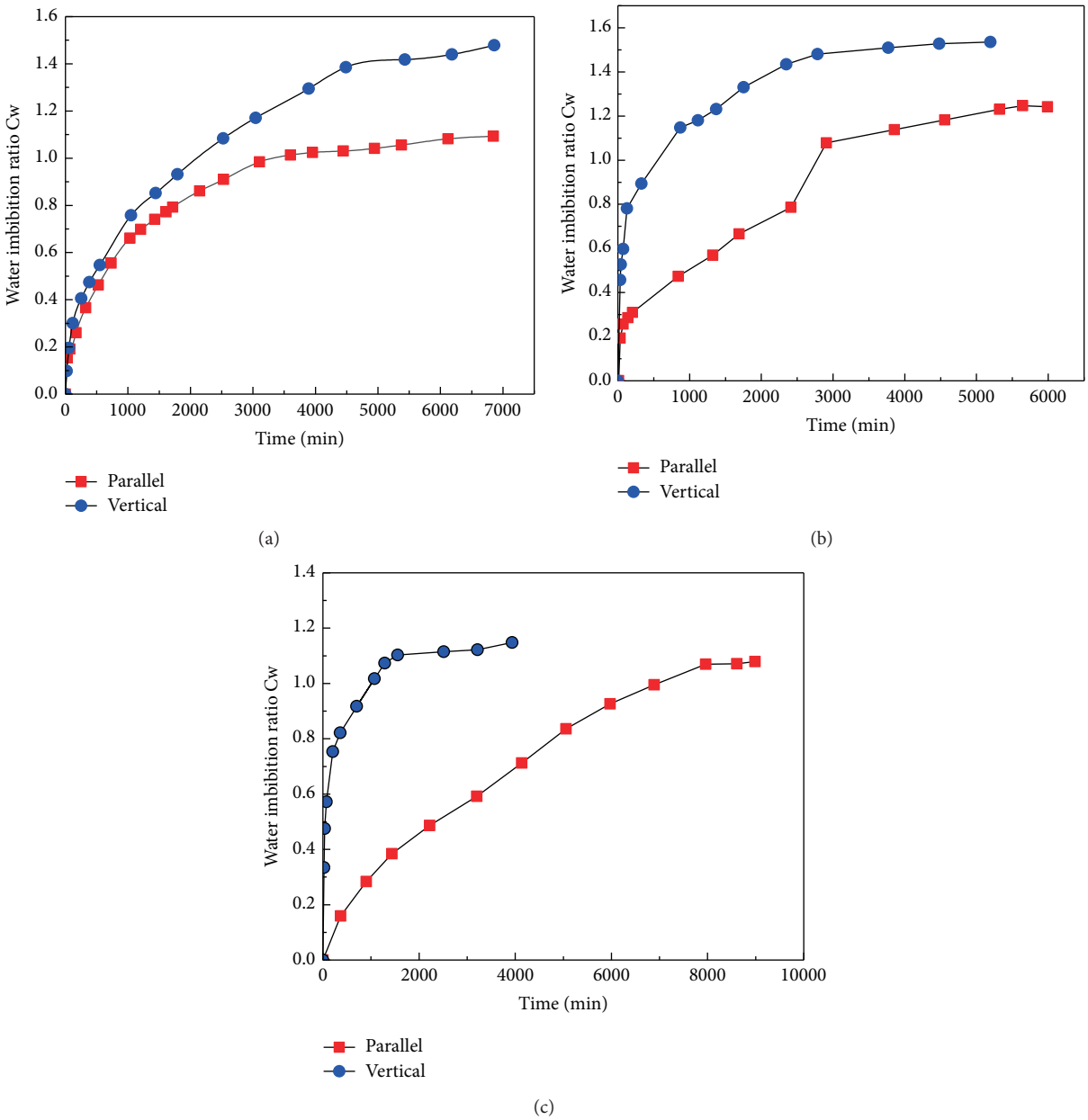

Figure 4: Comparison of water imbibition differences between vertical and parallel bedding directions of different lithofacies. (a) Sandy interlayer YY-72-2. (b) Low organic matter laminated siliceous shale YJ-62-3. (c) High organic matter laminated siliceous shale YA-151-1.

water imbibition curves of parallel bedding plane and vertical bedding plane of low organic matter laminated siliceous shale (YJ-62-3) and high organic matter laminated siliceous shale (YA-151-1). The sample has a very developed lamellar structure, which leads to great differences in the imbibition in different directions. It can be seen from Figures 4(b) and 4(c) that the rate of imbibition of vertical bedding plane is much greater than that of parallel bedding plane, and the

final water imbibition volume of vertical bedding plane is also greater than the final water imbibition volume of parallel bedding plane.

3.2.2. Differences in the Imbibition Characteristics of Oil and Water. Different lithofacies samples have differences in the oil and water imbibition rate, imbibition time, and final imbibition volume. For sandy interlayer (YY-72-2) and high organic matter laminated siliceous shale (YA-151-1), the oil imbibition rate is obviously greater than the water imbibition rate, and the final water imbibition volume is greater than oil. For low organic matter laminated siliceous shale (YJ-62-3), high organic matter massive siliceous shale (YD-22-1), and high organic matter massive clay shale (YJ-27-1), the initial oil imbibition rate is similar to the water imbibition rate, and the oil-water equilibrium time is also similar, but the final water imbibition is greater than that of the oil. The water imbibition rate of the low organic matter laminated siliceous shale (YG-616-3) is much greater than the oil imbibition rate, and the final water imbibition volume is much greater than oil. Figure 5(a) shows the comparison of the oil-water imbibition curve of the sandy interlayer sample (YY-72-2). It is observed from Figure 5(a) that the oil imbibition rate is greater than the water imbibition rate, but the water imbibition time is longer than the oil imbibition time. The final imbibition volume of water is greater than that of oil. Figure 5(b) shows the comparison of oil-water imbibition curves of the low organic matter laminated siliceous shale (YJ-62-3). It is observed from Figure 5(b) that the water imbibition rate is similar to the oil imbibition rate at the initial stage. There is little difference in the imbibition time, and the final imbibition volume of water is greater than that of oil. Figure 5(c) shows the comparison of oil-water imbibition curves of the high organic matter laminated siliceous shale sample (YA-151-1). It is observed from Figure 5(c) that the initial oil imbibition rate is greater than the water imbibition rate, but it is subsequently overtaken by water. The water imbibition time is longer than the oil imbibition time, and the final imbibition volume of water is greater than that of oil. Figure 5(d) shows the comparison of oil-water imbibition curves of high organic matter massive siliceous shale (YD-22-1). It is observed from Figure 5(d) that the water imbibition rate at the initial stage is similar to the oil imbibition rate, and the final imbibition volume of water is greater than that of oil. Figure 5(e) shows the comparison of oil-water imbibition curves of low organic matter laminated siliceous shale (YG-616-3). It can be observed from Figure 5(e) that the water imbibition rate is significantly greater than the oil imbibition rate, the oil imbibition time is longer than the water imbibition time, and the final imbibition volume of water is much greater than that of oil. Figure 5(f) shows the comparison of oil-water imbibition curves of high organic matter massive clay shale (YJ-27-1). It can be observed from Figure 5(f) that the water imbibition rate is similar to the oil imbibition rate at the initial stage, the oil imbibition time is longer than the water imbibition time, and the final imbibition volume of water is greater than that of oil.

The volume of oil imbibed by the sample is less than the pore volume; that is, the sample will not be excessively imbibed with oil. C_o is the percentage of the final oil imbibition volume to the pore volume, and the relationship of C_o between different lithofacies is as follows: high organic matter massive clay shale > high organic matter laminated siliceous shale > sandy interlayer > low organic matter laminated siliceous shale > high organic matter massive siliceous shale.

The volume of water imbibed by the sample is greater than the pore volume; that is, excessive water imbibition occurs in the sample. Capillary force is a physical action that occurs under the action of connected pores. If capillary force is the main driving force for water imbibition, the imbibition volume will be smaller than the pore volume. Therefore, the hydration of clay minerals is the cause of excessive imbibition of water by the sample. C_w is the percentage of the final water volume to the pore volume, and the C_w relationship of different lithofacies is as follows: low organic matter laminated siliceous shale > high organic matter massive clay shale > sandy interlayer > high organic matter laminated siliceous shale > high organic matter massive siliceous shale.

3.3. NMR Imbibition. Different lithofacies have different ways of oil imbibition. Sandy interlayer is simultaneously imbibed with large and tiny pores, and low organic matter laminated siliceous shale and high organic matter massive clay shale first infiltrate tiny pores and then large pores. The T2 spectrum peaks of the three different lithofacies samples of n-dodecane imbibed showed a relatively obvious shift to the right. In contrast, the T2 spectrum peaks of the imbibed deionized water did not appear to be significantly shifted to the right. This shows that most of the imbibed water is adsorbed water, and only a small amount of water becomes free-flowing water. Figures 6(a) and 6(b) show the imbibition characteristics of the sandy interlayer (YY-72-2). The imbibition rate of n-dodecane is of high speed, and the imbibition equilibrium is reached in only 1314 minutes, and almost the entire pore volume can be imbibed. There is little difference between the final oil imbibition and saturated oil. The imbibition method is simultaneous imbibition of tiny and large pores, and the T2 spectrum peak shifts to the right. The imbibition of water is slow, and the imbibition equilibrium can be reached at 6800 minutes. The amount of imbibition is large, but most of the water is adsorbed water, and only a tiny amount of water becomes free-flowing water, and the T2 spectrum peak does not appear to shift to the right. Figures 6(c) and 6(d) show the imbibition characteristics of low organic matter laminated siliceous shale (YJ-62-3). The n-dodecane imbibition rate is fast, and the imbibition equilibrium is reached at 2250 min. The oil imbibition is low, and it is not entirely imbibed, which is a certain gap between the results of the saturated oil. The imbibition method is to first imbibe tiny pores and then large pores, and the T2 spectrum peak shifts to the right. The imbibition rate of water is slow, reaching equilibrium at 4800 minutes. Almost all of the imbibed water is adsorbed water, only a

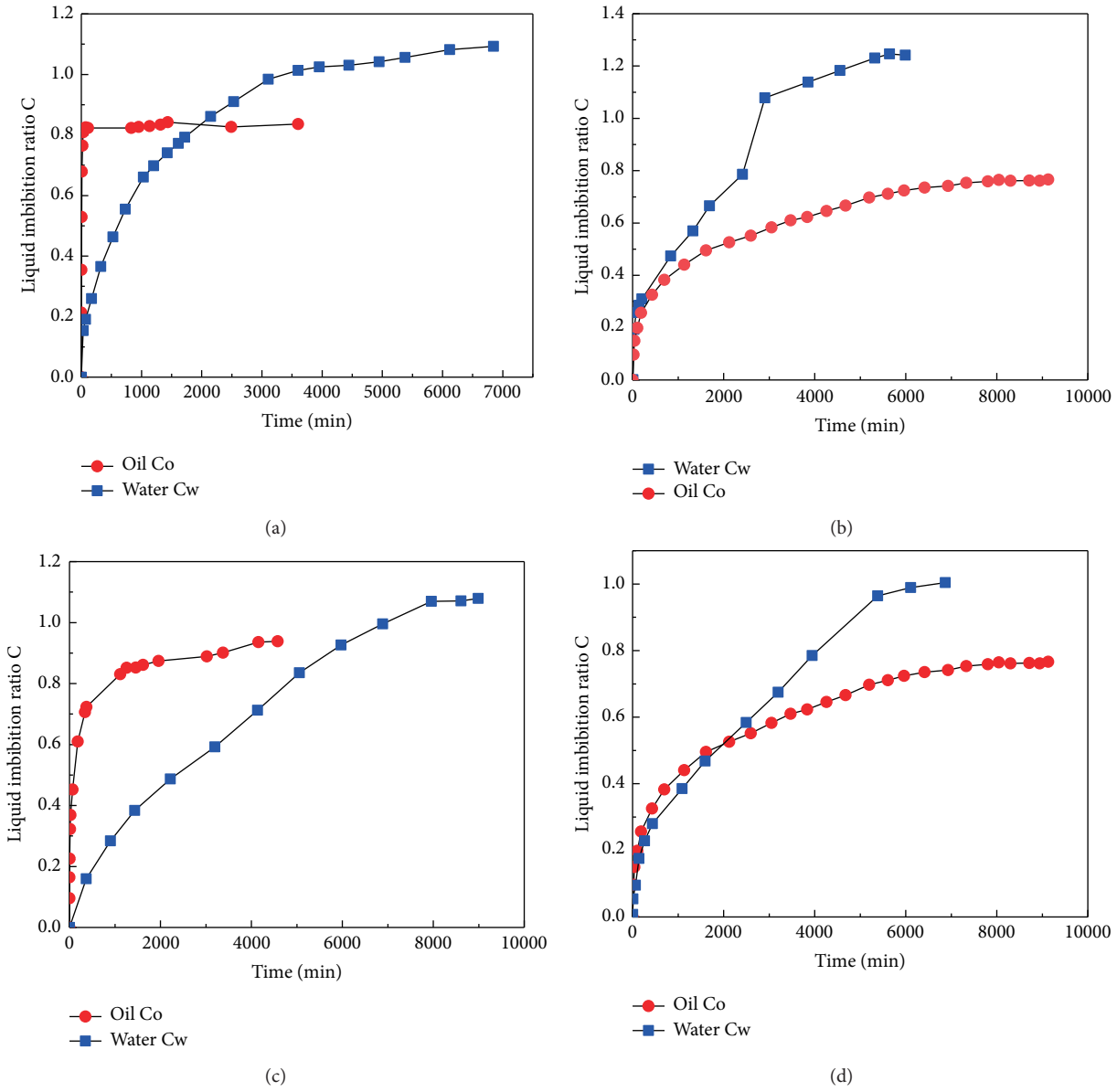

Figure 5: Continued.

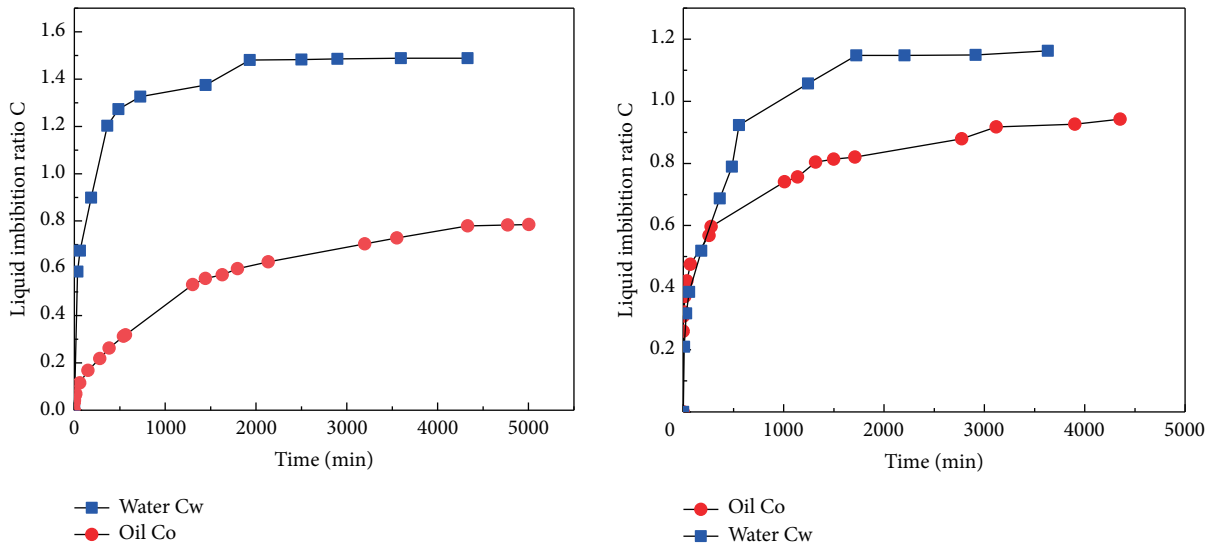

Figure 5: Differences in imbibition characteristics of n-dodecane and deionized water for different petrographic samples. (a) Sandy interlayer YY-72-2. (b) Low organic matter laminated siliceous shale YJ-62-3. (c) High organic matter laminated siliceous shale YA-151-1. (d) High organic matter massive siliceous shale YD-22-1. (e) Low organic matter laminated siliceous shale, YG-616-3. (f) High organic matter massive clay shale YJ-27-1.

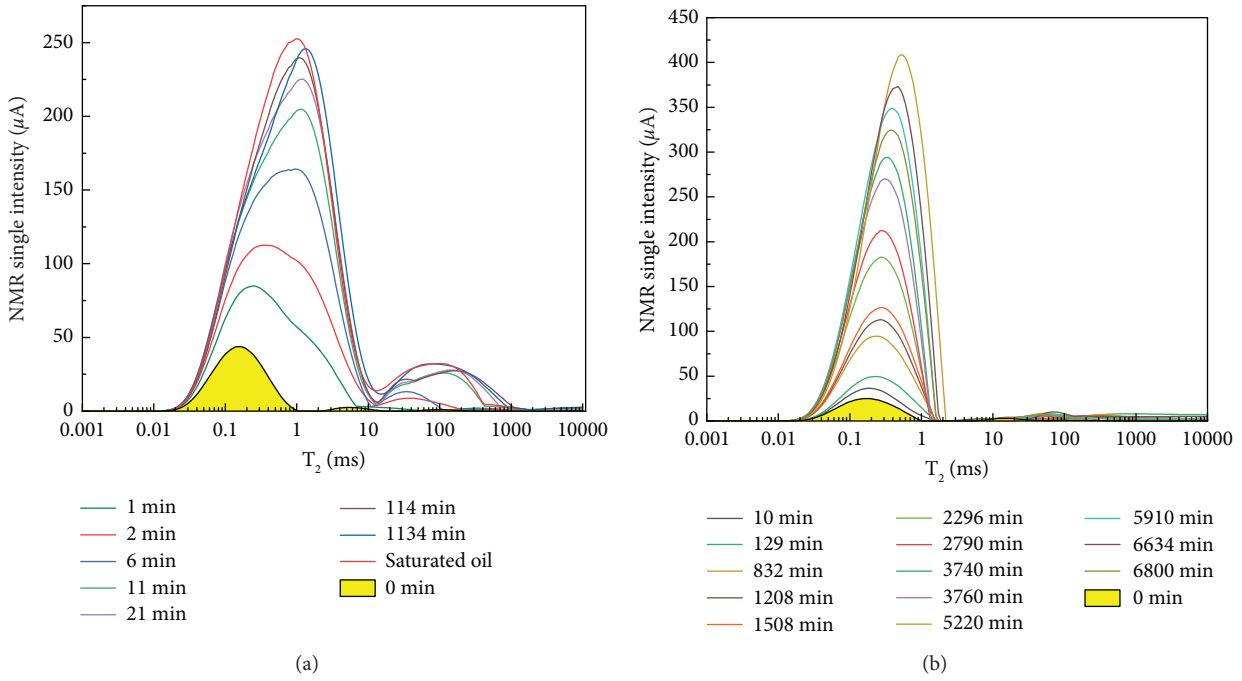

Figure 6: Continued.

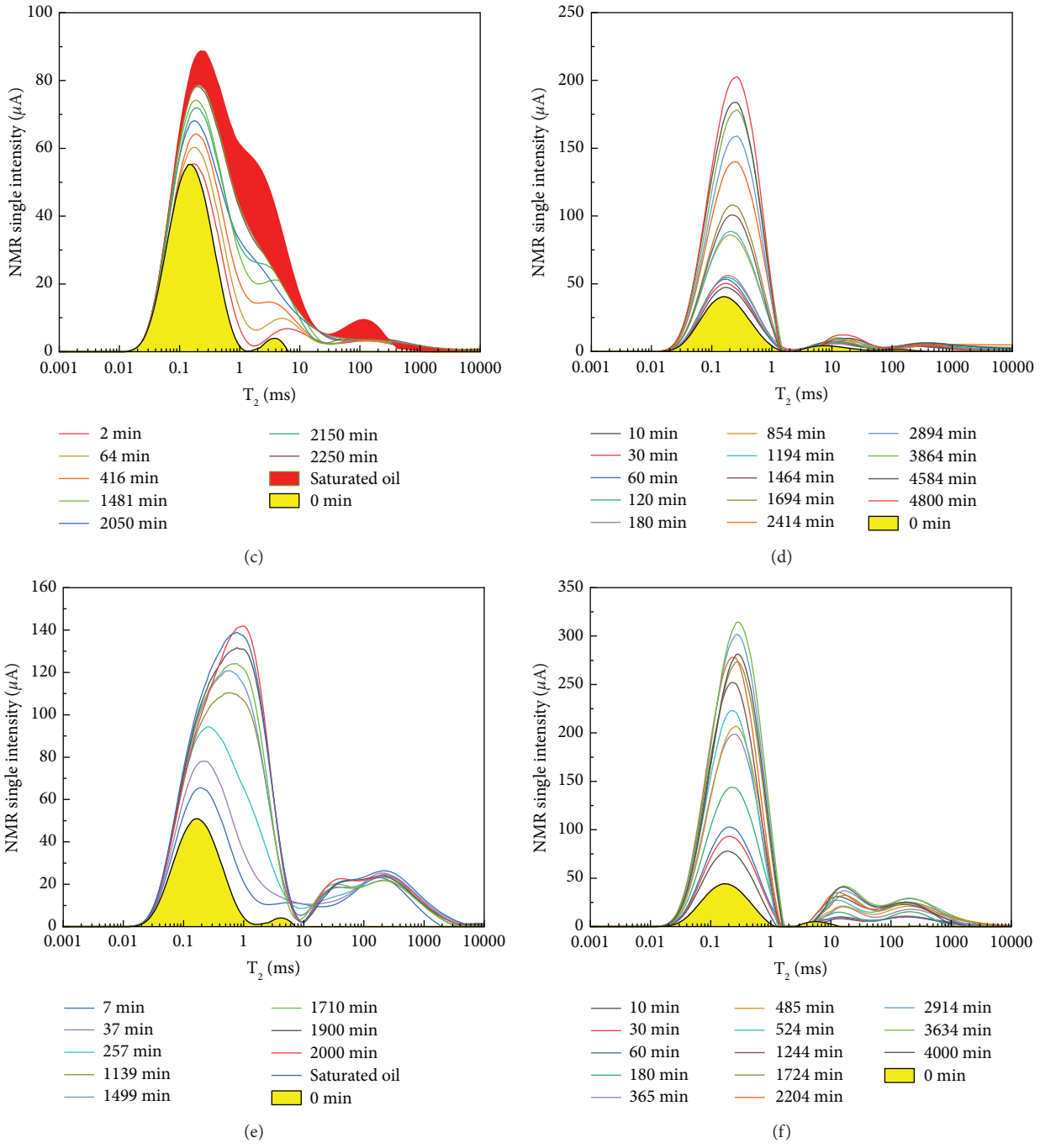

Figure 6: Microscopic characteristics of percolation of n-dodecane and water from different lithofacies samples. (a) Sandy interlayer oil imbibition YY-72-2. (b) Sandy interlayer water imbibition YY-72-2. (c) Low organic matter laminated siliceous shale oil imbibition YJ-62-3. (d) Low organic matter laminated siliceous shale water imbibition YJ-62-3. (e) High organic matter massive clay shale oil imbibition YJ-27-1. (f) High organic matter massive clay shale water imbibition YJ-27-1.

small part is free-flowing water, and the T2 spectrum peak does not appear to shift to the right. Figures 6(e) and 6(f) show the imbibition characteristics of high organic matter massive clay shale (YJ-27-1). The imbibition rate of n-dodecane is fast, the imbibition equilibrium is reached in 2000 min, and the oil imbibition is relatively high, which is almost the same as the imbibition result of saturated oil. The imbibition method is first to imbibe tiny pores and then imbibe large pores, and the T2 spectrum peak appears to move right shifts. The speed of water imbibition is slow, reaching equilibrium after 4000 minutes. Almost all the water imbibed is bound by clay minerals and capillary tubes. Only a small part is free-flowing water, and the T2 spectrum peak does not appear to shift to the right.

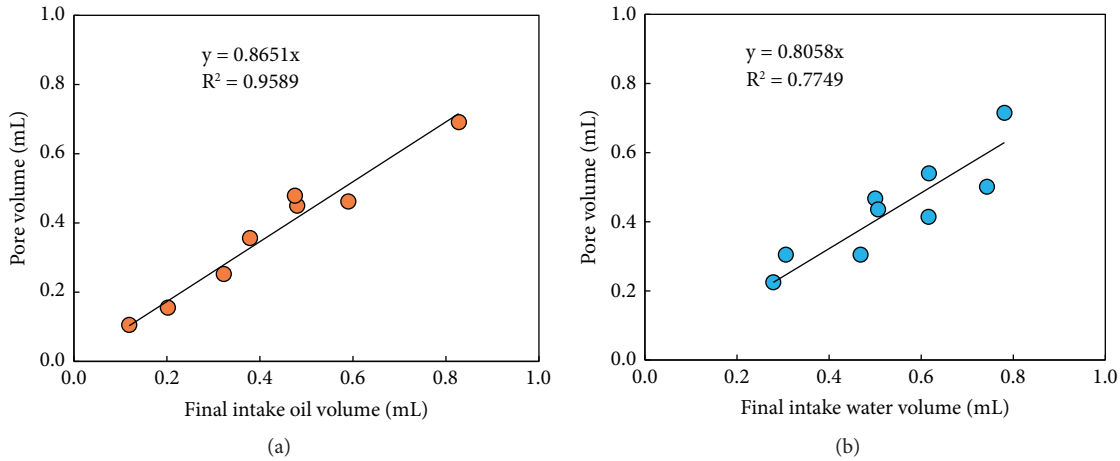

Figure 7: Correlation between imbibed liquid volume and pore volume. (a) Relationship between pore volume and oil imbibition volume. (b) Relationship between pore volume and water imbibition volume.

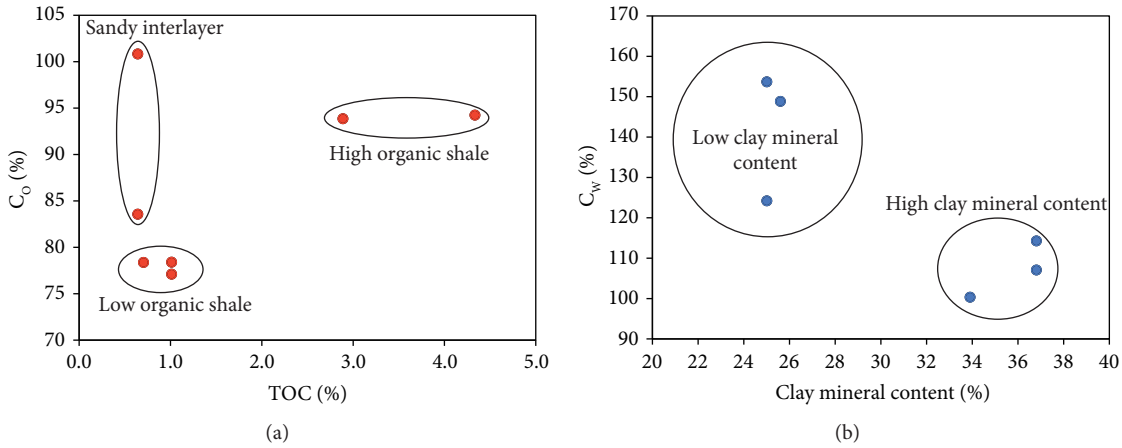

Figure 8: Relationship between TOC and clay minerals and oil-water imbibition. (a) Relationship between C_o and TOC. (b) Relationship between C_w and clay mineral content.

After the sample imbibed water, the T2 spectrum did not shift to the right; only the sandy interlayer shifted slightly to the right. The lower the degree of shift to the right, the weaker the core's ability to absorb water to produce microfractures. The water in the small pores does not flow to the large pores; that is, water lock is prone to occur, and the reservoir does not have the ability to "automatically relieve water lock." The relationship between the potentials of different lithofacies to "automatically release water lock" is as follows: Sandy interbeds > Low organic matter laminated siliceous shale > High organic matter massive clay shale. The stronger the water wetness, the greater the "potential for mitigating water lock."

3.4. Influencing Factors of Spontaneous Imbibition

3.4.1. Bedding Plane. For sandy interlayer, the difference between the imbibition of parallel bedding planes and vertical bedding planes is not significant. For shale, there is a certain difference between the imbibition of parallel bedding planes and the imbibition of vertical bedding planes. Regardless of the imbibition rate and the final imbibition amount, the imbibition along the bedding plane is greater than the imbibition along the vertical bedding plane. The reason is that ① the bedding plane has good connectivity; ② the water imbibition along the bedding plane is more likely to induce microcracks and further widen the microcracks. From this, we can conclude that, for shale intervals, the method of lateral fracturing and injecting fracturing fluid is better than that of longitudinal fracturing.

3.4.2. Pore Volume. Figures 7(a) and 7(b) show the relationship between pore volume and imbibition volume. Among them, V_o has a good correlation with pore volume, while V_w has a poor correlation with pore volume. The reason for this phenomenon is that shale contains certain clay minerals, and excessive water imbibition occurs in different lithofacies samples.

3.4.3. TOC and Clay Mineral Content. Figure 8(a) shows the relationship between C_o and TOC: the higher the TOC content of shale, the higher the C_o. This is because the higher

the TOC is, the more developed the lipophilic pore network will lead to the intake of oil. Figure 8(b) shows the relationship between C_w and clay mineral content: the higher the content of clay minerals, the lower the C_w. Clay minerals are the cause of excessive water imbibition in shale. When the clay minerals are too high, the shale will swell and block the pores due to water imbibition, which is not conducive to the further water imbibition of the shale.

4. Conclusions

(1) For the shale in this study area, whether n-dodecane or deionized water is imbibed, the imbibition rate and imbibition volume along the bedding plane are significantly greater than those along the vertical bedding plane. For sandy interlayers, the difference between parallel bedding plane imbibition and vertical bedding plane imbibition is not large. Therefore, in the shale oil development process, the method of lateral fracturing and injecting fracturing fluid is better than that of longitudinal fracturing.

(2) The water imbibition volume of the samples in this study area is greater than the pore volume: low organic matter laminated siliceous shale > high organic matter massive clay shale > sandy interlayer > high organic matter laminated siliceous shale > high organic matter massive siliceous shale. The higher the content of clay minerals, the lower the C_w. Clay minerals are the cause of excessive water imbibition in shale. When the clay minerals are too high, the shale will swell and block the pores due to water imbibition, which is not conducive to the further water imbibition of the shale.

(3) The oil imbibition volume of the samples in this study area is less than the pore volume: high organic matter massive clay shale > high organic matter laminated siliceous shale > sandy interlayer > low organic matter laminated siliceous shale > high organic matter massive siliceous shale. The higher the TOC content of shale, the higher the *Co*. This is because the higher the TOC, the more developed the lipophilic pore network, and the more oil will be imbibed.

(4) Nuclear magnetic experiments show that most of the water absorbed by the sample is adsorbed water, and the core has a poor ability to automatically relieve water lock. The relationship between the potentials of different lithofacies to "automatically release water lock" is as follows: sandy interbeds > low organic matter laminated siliceous shale > high organic matter massive clay shale. The stronger the water wetness, the greater the "potential for mitigating water lock."

Data Availability

The data used to support the findings of this study are available from the corresponding author upon request.

Conflicts of Interest

The authors declare that they have no conflicts of interest.

Authors' Contributions

Haitao Xue designed the project and wrote the main manuscript. Guozhi Ding helped in drawing the figures and drafting the manuscript. Zhentao Dong and Rixin Zhao defined the statement of problem. Ce An helped in discussing the problems and revising the manuscript. Guozhi Ding and Zhentao Dong helped in discussing the main idea and drafting the manuscript. Boheng Li and Yuan Zhou helped in calculating the data and drawing the figures. Penglei Yan, Jinliang Yan, Yuxi Jin, and Chunlei Li helped in revising the figures. All authors reviewed the manuscript.

Acknowledgments

This study was funded by the Sinopec Independent Innovation Fund (20200925145915002).

Supplementary Materials

Table S1. Quality change before and after imbibition of the n-dodecane sample. *Table S2.* Quality change before and after imbibition of the deionized water sample. *Figure S1.* Microscopic characteristics of percolation of n-dodecane and water for different petrographic samples. (a) Low organic matter laminated siliceous shale oil imbibition YG-616-3. (b) Low organic matter laminated siliceous shale water imbibition YG-616-3. (c) High organic massive siliceous shale oil imbibition YD-22-1. (d) High organic massive siliceous shale water imbibition YD-22-1. (e) High organic matter laminated siliceous shale oil imbibition YA-151-1. (f) High organic matter laminated siliceous shale water imbibition YA-151-1. (*Supplementary Materials*)

References

[1] F. Craig, "The reservoir engineering aspects of waterflooding, monograph series," *Society of Petroleum Engineers of AIME*, vol. 3, pp. 45–75, 1971.

[2] W. G. Anderson, "Wettability literature survey-part 1: rock/oil/brine interactions and the effects of core handling on wettability," *Journal of Petroleum Technology*, vol. 38, no. 10, pp. 1125–1144, 1986.

[3] M. Wang, R. Ma, J. Li et al., "Occurrence mechanism of lacustrine shale oil in the paleogene shahejie formation of Jiyang depression, Bohai Bay basin, China," *Petroleum Exploration and Development*, vol. 46, no. 4, pp. 833–846, 2019.

[4] Y. Lu, L. Zeng, A. Sari, Y. Chen, Y. Jin, and Q. Xie, "Wetting behavior of shale rocks and its relationship to oil composition," *Energy & Fuels*, vol. 33, no. 12, pp. 12270–12277, 2019.

[5] H. Roshan, A. Z. Al-Yaseri, M. Sarmadivaleh, and S. Iglauer, "On wettability of shale rocks," *Journal of Colloid and Interface Science*, vol. 475, pp. 104–111, 2016.

[6] Q. Xie, Y. Q. Chen, L. J. You, M. M. Hossain, and A. Saeedi, "Drivers of wettability alteration for oil/brine/kaolinite system: implications for hydraulic fracturing fluids uptake in shale rocks," *Energies*, vol. 11, no. 7, 2018.

[7] M. K. Dustin, J. R. Bargar, A. D. Jew et al., "Shale kerogen: hydraulic fracturing fluid interactions and contaminant release," *Energy & Fuels*, vol. 32, no. 9, pp. 8966–8977, 2018.

[8] L. P. Zeng, Y. Q. Chen, M. M. Hossain, A. Saeedi, and Q. Xie, "Wettability alteration induced water uptake in shale oil reservoirs: a geochemical interpretation for oil-brine-OM interaction during hydraulic fracturing," *International Journal of Coal Geology*, vol. 213, Article ID 103277, 2019.

[9] X. Sun, C. Dai, Y. Sun et al., "Wettability alteration study of supercritical CO_2 fracturing fluid on low permeability oil reservoir," *Energy & Fuels*, vol. 31, no. 12, pp. 13364–13373, 2017.

[10] M. A. Q. Siddiqui, X. Chen, S. Iglauer, and H. Roshan, "A multiscale study on shale wettability: spontaneous imbibition versus contact angle," *Water Resources Research*, vol. 55, no. 6, pp. 5012–5032, 2019.

[11] R. Dutta, C. H. Lee, S. Odumabo et al., "Experimental investigation of fracturing-fluid migration caused by spontaneous imbibition in fractured low-permeability sands," *SPE Reservoir Evaluation and Engineering*, vol. 17, no. 1, pp. 74–81, 2014.

[12] E. Odusina, C. Sondergeld, and C. Rai, "An NMR study on shale wettability," in *Proceedings of the Canadian Unconventional Resources Conference*, Calgary, Alberta, Canada, November 2011.

[13] E. C. Donaldson, R. D. Thomas, and P. B. Lorenz, "Wettability determination and its effect on recovery efficiency," *Society of Petroleum Engineers Journal*, vol. 9, no. 1, pp. 13–20, 1969.

[14] B. Bai, M. Elgmati, H. Zhang, and M. Wei, "Rock characterization of Fayetteville shale gas plays," *Fuel*, vol. 105, pp. 645–652, 2013.

[15] A. Kantzas, M. Pow, K. Allsopp, and D. Marentette, "Co-current and counter-current imbibition analysis for tight fractured carbonate gas reservoirs," in *Proceedings of the Technical Meeting/Petroleum Conference of the South Saskatchewan Section*, Regina, Canada, October 1997.

[16] C. R. Clarkson, F. Qanbari, and J. D. Williams-Kovacs, "Semi-analytical model for matching flowback and early-time production of multi-fractured horizontal tight oil wells," in *Proceedings of the SPE/AAPG/SEG Unconventional Resources Technology Conference*, San Antonio, TX, USA, August 2016.

[17] F. Javadpour, "Nanopores and apparent permeability of gas flow in mudrocks (shales and siltstone)," *Journal of Canadian Petroleum Technology*, vol. 48, no. 8, pp. 16–21, 2009.

[18] G. R. L. Chalmers and R. M. Bustin, "Geological evaluation of Halfway-Doig-Montney hybrid gas shale-tight gas reservoir, northeastern British Columbia," *Marine and Petroleum Geology*, vol. 38, no. 1, pp. 53–72, 2012.

[19] Z. Li, X. Yu, E. Xu, H. Jiang, B. Xi, and Q. Yang, "The characteristics of mineral components for effective source rocks from Dongying depression of Bohai Bay Basin and its significance," *Petroleum Geology and Experiment*, vol. 32, no. 3, pp. 270–275, 2010.

[20] M. E. Curtis, R. J. Ambrose, C. H. Sondergeld, and C. S. Rai, "Transmission and Scanning Electron Microscopy Investigation of Pore Connectivity of Gas Shales on the Nanoscale," in *Proceedings of the North American Unconventional Gas Conference and Exhibition*, The Woodlands, TX, USA, June 2011.

[21] S. Su, Z. Jiang, X. Shan et al., "The wettability of shale by NMR measurements and its controlling factors," *Journal of Petroleum Science and Engineering*, vol. 169, pp. 309–316, 2018.

[22] M. Xu and H. Dehghanpour, "Advances in understanding wettability of gas shales," *Energy & Fuels*, vol. 28, no. 7, pp. 4362–4375, 2014.

[23] F. P. Wang, U. Hammes, R. Reed, T. W. Zhang, X. H. Tang, and Q. H. Li, "Petrophysical and mechanical properties of organic-rich shales and their influences on fluid flow," *AAPG Memoir*, vol. 103, pp. 167–186, 2013.

[24] Z. Gao, Y. Fan, Q. Hu, Z. Jiang, Y. Cheng, and Q. Xuan, "A review of shale wettability characterization using spontaneous imbibition experiments," *Marine and Petroleum Geology*, vol. 109, pp. 330–338, 2019.

[25] M. D. Sun, J. L. Zhao, Z. J. Pan et al., "Pore characterization of shales: a review of small angle scattering technique," *Journal of Natural Gas Science and Engineering*, vol. 78, Article ID 103294, 2020.

[26] S. S. Tian, L. Bowen, B. Liu et al., "A method for automatic shale porosity quantification using an Edge-Threshold Automatic Processing (ETAP) technique," *Fuel*, vol. 304, Article ID 121319, 2021.

[27] B. Liu, Y. Gao, K. Liu et al., "Pore structure and adsorption hysteresis of the middle Jurassic Xishanyao shale formation in the Southern Junggar Basin, northwest China," *Energy Exploration and Exploitation*, vol. 39, no. 3, pp. 761–778, 2021.

[28] F. Zeng, C. M. Dong, C. Y. Lin et al., "Analyzing the effects of multi-scale pore systems on reservoir properties—a case study on Xihu depression, East China sea shelf basin, China," *Journal of Petroleum Science and Engineering*, vol. 203, Article ID 108609, 2021.

[29] H. Sharifigaliuk, S. M. Mahmood, W. Al-Bazzaz, and V. Khosravi, "Complexities driving wettability evaluation of shales toward unconventional approaches: a comprehensive review," *Energy & Fuels*, vol. 35, no. 2, pp. 1011–1023, 2021.

[30] M. Begum, M. R. Yassin, and H. Dehghanpour, "Effect of kerogen maturity on organic shale wettability: a Duvernay case study," *Marine and Petroleum Geology*, vol. 110, pp. 483–496, 2019.

[31] J. J. Sheng, "Discussion of shale rock wettability and the methods to determine it," *Asia-Pacific Journal of Chemical Engineering*, vol. 13, no. 6, 2018.

[32] T. Engelder, L. M. Cathles, and L. T. Bryndzia, "The fate of residual treatment water in gas shale," *Journal of Unconventional Oil and Gas Resources*, vol. 7, pp. 33–48, 2014.

[33] M. Mokhtari, A. A. Alqahtani, A. N. Tutuncu, and X. L. Yin, "Stress-dependent permeability anisotropy and wettability of shale resources," in *Proceedings of the SPE/AAPG/SEG Unconventional Resources Technology Conference*, Denver, CO, USA, August 2013.

[34] A. Borysenko, B. Clennell, R. Sedev et al., "Experimental investigations of the wettability of clays and shales," *Journal of Geophysical Research: Solid Earth*, vol. 114, no. B7, 2009.

[35] L. Liang, D. Luo, X. Liu, and J. Xiong, "Experimental study on the wettability and adsorption characteristics of Longmaxi formation shale in the Sichuan Basin, China," *Journal of Natural Gas Science and Engineering*, vol. 33, pp. 1107–1118, 2016.

[36] S. Takahashi and A. R. Kovscek, "Spontaneous countercurrent imbibition and forced displacement characteristics of low-permeability, siliceous shale rocks," *Journal of Petroleum Science and Engineering*, vol. 71, no. 1, pp. 47–55, 2010.

[37] H. Dehghanpour, H. A. Zubair, A. Chhabra, and A. Ullah, "Liquid intake of organic shales," *Energy & Fuels*, vol. 26, no. 9, pp. 5750–5758, 2012.

[38] K. Makhanov, H. Dehghanpour, and E. Kuru, "An experimental study of spontaneous imbibition in Horn River

shales," in *Proceedings of the SPE Canadian Unconventional Resources Conference*, Alberta, Canada, October 2012.

[39] F. M. Hum and A. Kantzas, "Using low-field NMR to determine wettability of, and monitor fluid uptake in, coated and uncoated sands," *Journal of Canadian Petroleum Technology*, vol. 45, no. 7, 2006.

[40] X. J. Wang, M. Wang, Y. Li et al., "Shale pore connectivity and influencing factors based on spontaneous imbibition combined with a nuclear magnetic resonance experiment," *Marine and Petroleum Geology*, vol. 132, Article ID 105239, 2021.

[41] B. Liu, J. Sun, Y. Zhang et al., "Reservoir space and enrichment model of shale oil in the first member of Cretaceous Qingshankou Formation in the Changling Sag, southern Songliao Basin, NE China," *Petroleum Exploration and Development*, vol. 48, no. 3, pp. 608–624, 2021.

[42] H. T. Xue, Z. T. Dong, S. S. Tian et al., "Characteristics of shale wettability by contact angle and its influencing factors: a case study in Songliao," *Frontiers of Earth Science*, vol. 9, Article ID 864, 2021.

[43] B. Liu, H. Wang, X. Fu et al., "Lithofacies and depositional setting of a highly prospective lacustrine shale oil succession from the Upper Cretaceous Qingshankou Formation in the Gulong sag, northern Songliao Basin, northeast China," *AAPG Bulletin*, vol. 103, no. 2, pp. 405–432, 2019.

[44] Z. H. Feng, W. Fang, Z. G. Li et al., "Depositional environment of terrestrial petroleum source rocks and geochemical indicators in the Songliao Basin," *Science China Earth Sciences*, vol. 54, no. 9, 2011.

[45] M. Yang, "Stratigraphic characteristics and geological significance of Qingshankou Formation in Songliao Basin," *IOP Conference Series: Earth and Environmental Science*, vol. 787, no. 1, Article ID 012097, 2021.

[46] Y. Chen, W. Xia, and G. Xie, "Contact angle and induction time of air bubble on flat coal surface of different roughness," *Fuel*, vol. 222, pp. 35–41, 2018.

[47] Z. Y. Gao and Q. H. Hu, "Wettability of Mississippian Barnett Shale samples at different depths: investigations from directional spontaneous imbibition," *AAPG Bulletin*, vol. 100, no. 1, pp. 101–114, 2016.

[48] Z. Shen and J. J. Sheng, "Experimental and numerical study of permeability reduction caused by asphaltene precipitation and deposition during CO_2 huff and puff injection in Eagle Ford shale," *Fuel*, vol. 211, pp. 432–445, 2018.